

Van Hove Singularities in disordered multichannel quantum wires and nanotubes

S. Hügler and R. Egger

Institut für Theoretische Physik, Heinrich-Heine-Universität, D-40225 Düsseldorf, Germany

(Date: May 21, 2019)

We present a theory for the van Hove singularity (VHS) in the tunneling density of states (TDOS) of disordered multichannel quantum wires, with particular focus on multi-wall carbon nanotubes. We assume close-by gates which screen off electron-electron interactions, leading to the picture of non-interacting random Dirac fermions on a cylinder. By using diagrammatic perturbation theory within a non-crossing approximation which is valid over a wide parameter region, we obtain closed analytical expressions governing the disorder-induced broadening and shift of VHS's as new subbands are opened. This problem is nontrivial because the (lowest-order) Born approximation breaks down close to the VHS. Interestingly, the boundary TDOS shows drastically altered VHS, even in the clean limit. The typical $1/\sqrt{E - E_n}$ dependence of the VHS turns into a $\sqrt{E - E_n}$ behavior close to the boundary, where E_n is the threshold energy.

I. INTRODUCTION

Van Hove singularities (VHS's) in the thermodynamic density of states (DOS) have been predicted in 1953¹ and were observed in many experiments since then. The DOS for a d -dimensional system with dispersion relation $E(\vec{k})$ is

$$\nu(E) = \int \frac{d\vec{k}}{(2\pi)^d} \delta(E - E(\vec{k})), \quad (1)$$

which can be rewritten as a surface integral over the Fermi surface,

$$\nu(E) = \int \frac{dS}{(2\pi)^d} \frac{1}{|\nabla_{\vec{k}} E(\vec{k})|}.$$

The quantity in the denominator is basically the group velocity. Due to symmetries in a crystal, the group velocity may vanish at certain momenta, resulting in a divergent integrand. This divergence is integrable in three dimensions, and typically leads to a finite DOS. In lower dimensions, however, very pronounced VHS appear. In this paper, we focus on the one-dimensional (1D) limit, where the VHS diverges like $\nu(E) \sim (E - E_n)^{-1/2}$ in a clean system when the energy E approaches the threshold E_n from above. Therefore VHS appear as sharp features in the energy-dependent DOS reflecting the onset of new active subbands. Similar VHS's exist for the tunneling density of states (TDOS) measured at some location x along the system,

$$\nu(E, x) = \frac{\text{Re}}{\pi\hbar} \int_0^\infty dt e^{iEt/\hbar} \langle \psi(x, t) \psi^\dagger(x, 0) \rangle,$$

where $\psi(x, t)$ is the electron field operator and the brackets denote a quantum expectation value. The TDOS is

easily accessible experimentally by measuring the conductance through a weak link or a tunnel junction. Typically, it is obtained by means of scanning tunneling spectroscopy (STS).^{2,3} In general, one has to carefully distinguish between the DOS and the TDOS. While the DOS is a thermodynamic property of the system, the TDOS is a local property and therefore depends on the position. In the “bulk” limit, the DOS and the (possibly coarse-grained) TDOS are expected to be identical, but near a boundary they can strongly differ.

In the present paper we try to answer the question: How is the VHS modified by the presence of disorder? This question is of importance for the interpretation of experiments on multi-wall nanotubes (MWNTs). Due to their intriguing electronic and mechanical properties, carbon nanotubes continue to attract much attention.⁴ While single-wall nanotubes (SWNTs) are ballistic 1D quantum wires⁵ with a Luttinger liquid phase due to electron-electron interactions,⁶ lately much effort, including this work, has been devoted to studying the electronic properties of MWNTs. A MWNT consists of a few concentrically arranged graphite shells, with a typical outermost-shell radius $R \approx 5$ to 20 nm and lengths of up to 1 mm. (For the figures shown below, we take $R = 10$ nm which is typical for arc-discharge grown tubes, but the general equations are of course valid for any R .) As demonstrated by magnetoresistance measurements,⁷ electronic transport occurs only through the outermost shell and exhibits the typical fingerprints of diffusive behavior. This can be rationalized since the incommensurate inner-shell ionic potential acts on electrons in the outermost shell, with the resulting quasi-periodic potential effectively acting as a random potential.^{8,9} The crucial difference between electronic transport in SWNTs and MWNTs therefore seems to come from the presence of disorder.

The observation of VHS's in recent STS experiments on SWNTs on a metallic substrate represents a direct proof for a 1D band structure.^{10–12} In particular, the predicted $1/\sqrt{E - E_n}$ behavior of ballistic 1D wires has been observed. We then need to understand how VHS's develop with increasing amounts of disorder. Reported

elastic mean free paths for MWNTs are in the range $l \approx 5$ to 100 nm (whereas metallic SWNTs can have l of the order of microns), but by intentionally damaging the tubes, e.g. by fast ion bombardment (FIB), any level of disorder may be realized experimentally to test our predictions below. For $l \gg R$, we have the situation of 1D ballistic transport (as observed in SWNTs), whereas 2D diffusive behavior is characterized by $l \ll R$. For typical MWNTs with $l \approx 2\pi R$, the characteristic subband features of the TDOS should still be present, albeit considerably broadened and possibly shifted. This question is clearly also of relevance to other quasi-1D quantum wires, such as long chain molecules.

Previous experiments on intrinsically (hole-) doped MWNTs (where $E_F \approx 0.5$ eV) reported by Bachtold *et al.*¹³ have observed power-law zero bias anomalies at low energy scales. These results have been explained in terms of electron-electron interactions in conjunction with diffusive motion, which effectively leads to a very efficient Coulomb blockade for tunneling into the MWNT.⁸ Due to the strong interactions, this power law can be thought of as a non-perturbative Altshuler-Aronov anomaly. Here we focus on a completely different scenario, where the electron-electron interaction is screened off by working on a metallic substrate. This is typical for STS measurements, which can directly probe the TDOS. For that reason, we omit interactions and treat only the non-interacting problem. Then spin only contributes trivial factors of two and is ignored henceforth. In particular, it will not affect the TDOS apart from the overall prefactor two. In addition, disorder-induced scattering between the two distinct gapless Fermi (K) points of the first Brillouin zone of the honeycomb lattice⁴ should be largely suppressed for reasons given below, and we thus consider only one Fermi point. It should be stressed that in typical STS experiments, only the TDOS of the outermost shell is probed. In the following, an effective single-shell model is assumed, where inner shells only give rise to a disorder potential for electrons on the outermost shell. We are then left with the problem of determining the TDOS for (one species of) non-interacting disordered Dirac fermions on the cylinder. As we show below, an approximate yet accurate analytical solution to this problem can be given. The corresponding problem on the plane is related to other applications, e.g. disordered d -wave superconductors or quantum Hall transitions, and has been addressed before by many authors.^{14–18} However, the techniques used in these papers do not allow to directly address the question of relevance here, since they appear to be restricted to the true 2D limit.

The outline of this paper is as follows. In Sec. II we describe the model and discuss the various disorder mechanisms, followed by an exact computation of the local TDOS for the clean case in Sec. III. In Sec. IV we treat the disordered case using diagrammatic perturbation theory for the important case of potential scattering. The results are then discussed in Sec. V and, finally, we give some conclusions in Sec. VI.

II. MODEL

Nanotubes are tubular nanoscale objects which can be thought of as graphite sheets wrapped onto a cylinder. Using $\vec{k} \cdot \vec{p}$ theory for the honeycomb lattice, one can establish that the effective low-energy theory of a *clean* graphite sheet is given by the 2D Dirac Hamiltonian.¹⁹ This graphite sheet is rolled up into a tube by enforcing periodic boundary conditions around the y direction, the tube pointing along the x direction. The action of the resulting system can be interpreted as the action of an equivalent quantum problem in $(1+1)$ dimensions, $(x, y) \rightarrow (x, \tau)$, with y playing the role of imaginary time τ . Under this correspondence, the circumference of the outermost shell maps to the “temperature” of the quantum system,

$$\beta^{-1} = k_B T_{\text{eff}} = \frac{\hbar v_F}{2\pi R}. \quad (2)$$

However, the physical temperature is always taken as zero in this study. We note that the Fermi velocity in nanotubes is $v_F = 8 \times 10^5$ m/s, but in order to simplify notation, we set $\hbar = v_F = 1$ from now on.

The arrangement of carbon atoms on the tube surface is determined by the integer indices $0 \leq s \leq r$ of the wrapping superlattice vector $\vec{T} = r\vec{a}_1 + s\vec{a}_2$, where \vec{a}_1 and \vec{a}_2 are the primitive Bravais translation vectors of the honeycomb lattice of length $a = \sqrt{3}d \approx 2.46$ Å, with the C-C nearest-neighbor distance d . The radius of the tube is then simply given by $R = |\vec{T}|/2\pi = a\sqrt{r^2 + s^2 + rs}/2\pi$. In the absence of disorder, electrons on the outermost shell are then described by the Dirac Hamiltonian

$$H_0 = \frac{1}{\beta} \sum_n \int \frac{dk}{2\pi} \psi^\dagger(\vec{k}) (\vec{\sigma} \cdot \vec{k} + M\sigma_y) \psi(\vec{k}), \quad (3)$$

with $\vec{k} = (k, \omega_n)$ and the “Matsubara frequencies” $\omega_n = 2\pi n/\beta$ with integer n due to the finite radius, see Eq. (2). ψ is a two-component spinor, where the two components reflect the sublattice degree of freedom, as the honeycomb lattice has a basis containing two atoms. Correspondingly, the Pauli matrices $\vec{\sigma} = (\sigma_x, \sigma_y)$ act in this sublattice space. Albeit the mass M is zero for a 2D graphite sheet, it can be nonzero for nanotubes due to chirality effects or an applied magnetic field parallel to the tube axis. In general, a flux Φ (in units of the flux quantum) gives rise to a mass $M = 2\pi\Phi/\beta$. Chirality effects in a (r, s) -tube cause a flux $\Phi_1 = -(2r+s)/3$.²⁰ A magnetic field B applied parallel to the tube axis causes an additional flux $\Phi_2 = B/B_0$ with $B_0 = h/\pi R^2 e$. (For a tube with $R = 10$ nm, for example, we have $B_0 = 13.2$ T.) Since the total flux is given by the sum of the two contributions, it is clear that chirality effects can always be absorbed by an appropriate adjustment of the magnetic field parallel to the tube, and therefore we consider

only the case $\Phi_1 = 0$. The mass term in Eq. (3) couples in the same way as $k_y = \omega_n$, and hence we can replace

$$\omega_n \rightarrow \omega_n + 2\pi\Phi_2/\beta = (n + B/B_0)/R \quad (4)$$

in Eq. (3) in order to include the mass term. Since n is integer, it is clear that for integer Φ_2 , the system is not influenced by the magnetic field, as we can simply shift n to absorb Φ_2 .

Next we discuss the various disorder mechanisms. In principle, for an effective low-energy theory, three types of randomness should be considered,

$$H_A = \int d\vec{x} \psi^\dagger(\vec{x}) \vec{\sigma} \cdot \vec{A}(\vec{x}) \psi(\vec{x}) , \quad (5)$$

$$H_{\tilde{V}} = \int d\vec{x} \tilde{V}(\vec{x}) \psi^\dagger(\vec{x}) \sigma_z \psi(\vec{x}) , \quad (6)$$

$$H_V = \int d\vec{x} V(\vec{x}) \psi^\dagger(\vec{x}) \psi(\vec{x}) , \quad (7)$$

where the fields \vec{A} , \tilde{V} , and V are random in space but constant in time. These three random fields are assumed to have zero mean, $\langle O(\vec{x}) \rangle = 0$, and a Gaussian white noise distribution for the fluctuations, $\langle O(\vec{x}) O(\vec{x}') \rangle = \Delta_O \delta(\vec{x} - \vec{x}')$, where Δ_O is the disorder strength for the field O corresponding to \vec{A} , \tilde{V} , and V , respectively. Focussing on disorder contributions of the inner-shell potentials, we can expand these fields in terms of reciprocal lattice vectors \vec{G} of the inner shells. Note that these are different from the ones of the outermost shell, since inner shells have different radii and chiralities. In particular, to obtain sizeable scattering between the two K points, the Fourier component of these random fields at $\vec{G} = 2\vec{K}$ should be finite. As $2\vec{K}$ is normally not an allowed reciprocal lattice vector on inner shells, scattering between the two distinct K points is expected to be drastically suppressed, as asserted above. From this observation, we then restrict ourselves to the single-K-point problem.

Let us now comment on the physical significance of these three terms. The contribution H_A describes a random vector potential caused by indirect hopping between nearest-neighbor sites on the honeycomb lattice via real or virtual states provided by the inner-shell ionic potential. Since hopping connects different sublattices, the resulting modulation of the hopping matrix element leads to the *random gauge field* $\vec{A}(\vec{x})$. Gauge field disorder also captures the effects of topological defects in the outermost shell.¹⁷ Both $H_{\tilde{V}}$ and H_V correspond to a random chemical potential. They arise from direct impurity potential scattering processes that are diagonal in sublattice space. The potential \tilde{V} is short-ranged and resolves the sublattice structure. In contrast, V is long-ranged and therefore does not distinguish between different sublattices. Using the standard replica trick to average over disorder, the two kinds of potential scattering can be mapped onto each other with the correspondence $\Delta_{\tilde{V}} \leftrightarrow -\Delta_V$.¹⁵ Here we focus only on H_V , since the \tilde{V}

term is, technically speaking, irrelevant under a renormalization group (RG) procedure. In particular, when the MWNT is intrinsically damaged by FIB, the dominant disorder mechanism is due to H_V .

In addition to the bulk case, we also address the *boundary TDOS* arising when one tunnels into the end of a MWNT. In reality, the end TDOS could of course be quite complex due to the formation of bound states. A few lattice spacings away from the end, however, we expect that the situation can be described by a continuum model, where bound state effects are negligible. Surprisingly, the presence of a boundary implies a drastic change in the TDOS despite the absence of electron-electron interactions, namely a strong suppression of the energy-dependent TDOS close to the boundary even in the absence of disorder, as will be shown below. For the subsequent calculations, we use the Greens function formalism. Here the TDOS reads

$$\nu(E, x) = -\frac{\text{Im}}{\pi} \text{Tr}_{\vec{k}, \sigma} G(E, \vec{k}, x), \quad (8)$$

where we have to trace over the “spin” coordinate (sublattice space), and over momentum using

$$\text{Tr}_{\vec{k}} = \sum_n \int_{-\infty}^{\infty} \frac{dk}{2\pi}.$$

Prefactors in the Greens function G are always chosen in order to recover the correct 1D normalization for the clean TDOS in the single-channel limit. Further, due to the symmetry of the TDOS, $\nu(-E) = \nu(E)$, within our model, we consider only $E > 0$.

III. DENSITY OF STATES IN THE CLEAN CASE

Before treating the disordered case, we first analyze the TDOS of a clean tube, see also Ref. 21. To be able to calculate both bulk and boundary TDOS, we study a semi-infinite ($x \geq 0$) tube, assuming a hard-wall potential at the boundary $x = 0$. This leads to the expansion

$$\psi(x, \tau) = \frac{1}{\beta} \sum_n \int_0^\infty \frac{dk}{\pi} \sin(kx) e^{i\omega_n \tau} \psi(k, \omega_n). \quad (9)$$

Using this expansion, the Greens function for energy $E > 0$ is

$$G_0(E, \vec{k}, x) = \frac{2 \sin^2(kx)}{E - \vec{\sigma} \cdot \vec{k} + i0^+}, \quad (10)$$

and hence the TDOS (8) reads

$$\begin{aligned} \frac{\nu(E, x)}{\nu_{1D}} &= 2|E| \\ &\times \sum_{n=-\infty}^{\infty} \frac{\sin^2(x\sqrt{E^2 - \omega_n^2})}{\sqrt{E^2 - \omega_n^2}} \Theta(E^2 - \omega_n^2), \end{aligned} \quad (11)$$

where Θ is the Heaviside step function. Throughout the paper, we use $\nu_{1D} = 1/\pi\hbar v_F$ as natural unit for the TDOS (without spin and K point degeneracy). Result (11) can be readily checked from the dispersion relation for Dirac fermions, $E(\vec{k}) = \sqrt{k^2 + \omega_n^2}$, by using the alternative Greens function

$$\bar{G}_0(E, \vec{k}, x) = \frac{2 \sin^2(kx)}{E - E(\vec{k}) + i0^+}$$

instead of Eq. (10). As one can see from Eqs. (11) and (4), the system can be gapped in the presence of a magnetic field B parallel to the tube axis. This gap can be changed as a function of B , and the system periodically becomes gapless with period B_0 .

Letting $x \rightarrow \infty$, with $\sin^2(x\sqrt{E^2 - \omega_n^2}) \rightarrow 1/2$, we obtain the *bulk TDOS*

$$\frac{\nu_0(E)}{\nu_{1D}} = |E| \sum_n \frac{\Theta(E^2 - \omega_n^2)}{\sqrt{E^2 - \omega_n^2}}, \quad (12)$$

which gives a constant and finite value (in the absence of a gap) for $E \rightarrow 0$, since then only $n = 0$ is possible. The bulk TDOS is equal to the thermodynamic DOS in this case. Clearly, the typical $1/\sqrt{E - \omega_n}$ VHS's of 1D systems appear at the onset of new subbands, $E = \omega_n$, see Fig. 1. (In all figures of this paper, $R = 10$ nm, but qualitatively similar findings were obtained for other R as well.) Depending on the strength of the magnetic field applied parallel to the tube axis, the system can be gapped or not. The pattern is periodic with period B_0 . Since the summation also includes negative values of n , the magnetic field causes a doubling of the VHS's, see Eq. (4) and Fig. 1.

Near the boundary, however, we obtain a completely different picture than predicted by the standard VHS of the thermodynamic DOS. Expanding the sine in Eq. (11) leads to the *boundary TDOS*

$$\frac{\nu_{\text{end}}(E, x)}{\nu_{1D}} = 2x^2 |E| \sum_n \Theta(E^2 - \omega_n^2) \sqrt{E^2 - \omega_n^2}. \quad (13)$$

For $E \rightarrow 0$, this predicts $\nu(E) \sim E^2$ for $B = 0$, in contrast to the finite boundary TDOS for a doped tube. This behavior can be traced back to the linear dispersion relation of Dirac fermions. More interestingly, the typical 1D VHS of the bulk TDOS is drastically altered close to the boundary. Instead of a divergence, the only sign of the opening of new subbands is a nonanalyticity at the threshold energy, with a *square-root energy dependence of the boundary TDOS* above the threshold, see Fig. 1. This possibly explains the observation of Ref. 12, where no divergencies were found in the tunneling spectrum at the end of a SWNT. However, to the best of our knowledge, the predicted square-root nonanalyticities of the end TDOS were not unambiguously observed so far. Nevertheless, the phenomenon is quite general. The exponent of the energy dependence of the TDOS close to a

given VHS changes by one if we go from the bulk to the boundary limit, for both Dirac and Schrödinger fermions. In the limit $E \rightarrow 0$, however, there is a difference. For Dirac fermions, the exponent changes by two, whereas for Schrödinger fermions, the exponent still changes only by one.

The crossover scale between bulk and boundary behavior of the TDOS depends on the energy. Focussing on E close to but above a given threshold energy ω_n , this scale is

$$x^* \approx \frac{\hbar v_F}{\sqrt{E^2 - \omega_n^2}}. \quad (14)$$

At zero temperature, the bulk limit is reached for $x \gg x^*$, and the boundary limit for $x \ll x^*$. Because of the energy dependence of x^* , one could effectively use E to tune from the bulk to the boundary limit for a given position x . For finite temperatures T , if the thermal scale $x_T = \hbar v_F/k_B T$ is smaller than x^* , one should replace x^* by x_T .

IV. DISORDERED CASE: NON-CROSSING APPROXIMATION

In this section, we compute the TDOS of a disordered MWNT using diagrammatic perturbation theory.²² We will consider only the effects of static disorder as introduced in Sec. II. Often, disorder has a profound influence on transport properties but only weakly affects the TDOS. The latter is no longer true, however, if the TDOS of the clean system vanishes linearly, $\nu(E) \sim |E|$, as is the case for 2D Dirac fermions, e.g. for a graphite sheet or a 2D d-wave superconductor.^{14,15} In the latter case, the standard procedure of averaging over disorder is complicated by the appearance of logarithmic singularities in the perturbative expansion of the single-electron self energy. The lowest-order Born approximation, see Fig. 2, is given by¹⁴ $\hat{\Sigma}^{(1)}(E) \sim E \ln |E|$. The second-order rainbow diagram, which is obtained by first-order renormalization of the internal electron line, contains an even stronger singularity, $\hat{\Sigma}_1^{(2)}(E) \sim E \ln^2 |E|$. The diagram with crossing impurity lines corresponds to a vertex renormalization in the Born self energy diagram, leading to the same singularity as the rainbow diagram. In fact, logarithmic singularities appear in all orders of perturbation theory including crossing diagrams. Therefore, in the 2D case, crossing diagrams must be treated on the same footing as the rainbow ones. In addition, in the single-channel 1D limit, it is also well known that crossed diagrams may be important. Since MWNTs are in between the 1D and the 2D limit, a careful study of the importance of crossed diagrams is therefore mandatory.

As we will show in this section, the situation for MWNTs is quite different from the 2D situation described above. First, there are *no logarithmic singularities* appearing in the self energy expansion. Second, the situ-

ation is further simplified by the fact that crossed diagrams are suppressed compared to the rainbow ones over a wide parameter and energy range of practical interest. Therefore we are entitled to compute the TDOS in a non-crossing approximation (NCA). We focus on the bulk case here and briefly comment on the boundary result at the end. Instead of Eq. (10), we then have

$$G_0(E, \vec{k}) = \frac{1}{E - \vec{\sigma} \cdot \vec{k} + i0^+}. \quad (15)$$

We start by looking at the self energy to lowest order in the disorder strength (Born approximation). The corresponding diagram is depicted in Fig. 2. Considering standard potential scattering (7), a scalar model emerges, where the impurity averaging procedure²² gives

$$\hat{\Sigma}_V^{(1)}(E) = \Delta_V \text{Tr}_{\vec{k}, \sigma} G_0(E, \vec{k}). \quad (16)$$

Using Eq. (15) and the Cauchy identity $1/(x + i0^+) = \mathcal{P}/x - i\pi\delta(x)$, one observes that the principal parts value vanishes, and we have

$$\hat{\Sigma}_V^{(1)}(E) = -i\pi\Delta_V\nu_0(E), \quad (17)$$

with $\nu_0(E)$ given in Eq. (12). If instead we consider the gauge field disorder (5), we have to deal with a vector model, leading to additional factors σ_μ at each vertex,

$$\hat{\Sigma}_A^{(1)}(E) = \Delta_A \text{Tr}_{\vec{k}, \sigma} \sum_{\mu=x,y} \sigma_\mu G_0(E, \vec{k}) \sigma_\mu.$$

As one can easily check, the result is just the same as for standard potential scattering besides an overall factor of 2 due to the “spin” degree of freedom, $2\hat{\Sigma}_V^{(1)}(E) = (\Delta_V/\Delta_A)\hat{\Sigma}_A^{(1)}(E)$. If we restrict ourselves to rainbow diagrams for the moment, the N th order for the scalar model is simply given by

$$\hat{\Sigma}_V^{(N)}(E) = \Delta_V^N \text{Tr}_{\{\vec{k}_i\}, \sigma} G_0^2(\vec{k}_1) \dots G_0^2(\vec{k}_{N-1}) G_0(\vec{k}_N).$$

Using $G_0^2 = -\partial_E G_0$, we arrive at

$$\hat{\Sigma}_V^{(N)}(E) = \hat{\Sigma}_V^{(1)}(E)(-\partial_E \hat{\Sigma}_V^{(1)}(E))^{N-1}. \quad (18)$$

Apart from the overall factor of 2, the same result is again found for the vector model. Within NCA, the special type of disorder is therefore not important. However, it could well be that crossed diagrams are important for the vector model, while we can establish the validity of NCA only for the scalar model (standard potential scattering). Since the latter is expected to represent the dominant disorder mechanism in MWNTs, we shall focus on the scalar model in what follows. Then a single dimensionless parameter Δ serves as a measure for the disorder strength, with $\Delta = \Delta_V R/\hbar^2 v_F^2$. Importantly, following our analysis, it is not possible to simply assume an energy-independent mean free path for all energies. Since

the disorder-averaged Greens function satisfies the Dyson equation,

$$G^{-1} = G_0^{-1} - \hat{\Sigma}, \quad (19)$$

we have an energy-dependent mean free time defined by $-\text{Im}\hat{\Sigma}(E) = \hbar/2\tau(E)$, and therefore an energy-dependent mean free path $l(E) = v_F\tau(E)$.

Next we address the breakdown of the Born approximation in the vicinity of a VHS. If we look at the second-order rainbow diagram in Fig. 2, which from Eqs. (18) and (17) is given by

$$\hat{\Sigma}_1^{(2)}(E) = (\pi\Delta)^2\nu_0(E)\partial_E\nu_0(E), \quad (20)$$

we see that the Born approximation must break down close to a VHS since

$$\left| \frac{\hat{\Sigma}_1^{(2)}(E)}{\hat{\Sigma}_1^{(1)}(E)} \right| = \pi\Delta\partial_E\nu_0(E).$$

The r.h.s. diverges for E approaching the threshold ω_n from above. We therefore must address the higher-order contributions to the self energy. For the moment, we shall assume that one can neglect all crossed diagrams. The justification for this will be given *a posteriori* at the end of this section. We can then treat the problem within NCA. Even within NCA, since the perturbation expansion is asymptotic, the problem is to arrange the order of summation in a physically meaningful way.

We propose an iterative approach similar to the one used by Lee²³ to calculate the TDOS of the disordered system. To this end, let us define the self energy in N th order for $N \geq 1$ as

$$\hat{\Sigma}^{(N)}(E) = \Delta \text{Tr}_{\vec{k}, \sigma} G_{N-1}(E, \vec{k}), \quad (21)$$

with the corresponding Dyson equation

$$G_N^{-1}(E, \vec{k}) = G_0^{-1}(E, \vec{k}) - \hat{\Sigma}^{(N)}(E). \quad (22)$$

This form is then used to calculate the self energy in $(N+1)$ th order. In each order, an average over disorder is performed, and the resulting Greens function is then employed to calculate the next order. It should be noted that under a direct summation along the lines of Eq. (18), familiar but unphysical divergencies appear, in particular when analyzing crossed diagrams, see Ref. 22. A correct treatment therefore requires an appropriate resummation technique such as the one employed here.

In the limit $N \rightarrow \infty$, this procedure converges and leads to the equation

$$\hat{\Sigma}(E) = \Delta \text{Tr}_{\vec{k}, \sigma} \frac{1}{G_0^{-1}(E, \vec{k}) - \hat{\Sigma}(E)}, \quad (23)$$

which has to be solved self-consistently for the self energy. The intuitive and physically appealing form of this result

gives further support to our resummation approach. The result for $\hat{\Sigma}(E)$ can then be used to compute the TDOS,

$$\nu(E) = -\frac{\text{Im}}{\pi\Delta}\hat{\Sigma}(E) \quad (24)$$

where we used Eq. (23).

Next we address the role of crossed diagrams. From the procedure outlined above, let us assume that we have constructed a proper Greens function (19) which includes the effects of all non-crossed diagrams. We now check that the effect of the simplest crossed diagram, see Fig. 2, is small compared to the self energy for the corresponding rainbow diagram in this order. For computational simplicity, we consider Schrödinger fermions, with the same conclusions expected also for Dirac fermions, especially in the vicinity of the VHS, where the Born approximation breaks down. The lowest-order crossed diagram is then given by

$$\hat{\Sigma}_2^{(2)}(\vec{k}_0, E) = \Delta^2 \text{Tr}_{\vec{k}, \vec{k}'} \bar{G}(\vec{k}) \bar{G}(\vec{k} + \vec{k}') \bar{G}(\vec{k}_0 + \vec{k}'), \quad (25)$$

where \vec{k}_0 is the external momentum, $\bar{G}^{-1} = E - E(\vec{k}) - \hat{\Sigma}$, and $E(\vec{k}) = \vec{k}^2/2m$. The dominant contribution to Eq. (25) comes from $|\vec{k}| \approx |\vec{k}_0| \approx |\vec{k} + \vec{k}'| \approx |\vec{k}_0 + \vec{k}'| = E/v_F$. Therefore, only $k' \approx 0$ and $n' = 0$ give an appreciable contribution to the crossed self energy. (There is a small contribution from $\vec{k}' = -2\vec{k}_0$, but due to its small phase space, $k' \approx 0$ is much more important.) Accordingly, we can neglect terms proportional to k'^2 , and a careful analysis of the pole structure leads to

$$\begin{aligned} \hat{\Sigma}_2^{(2)} &\approx i \frac{\Delta^2}{2\pi} \frac{m}{k_0} \text{Tr}_{\vec{k}} \bar{G}(\vec{k}) \\ &\times \frac{\Theta(-k_0 k) \text{sgn}(k_0)}{[E - E(\vec{k}_0) - \hat{\Sigma}]k/k_0 - [E - E(\vec{k}) - \hat{\Sigma}]} \end{aligned} \quad (26)$$

To estimate the contribution to the TDOS, one has to add external propagators $\bar{G}(\vec{k}_0)$. In the presence of these external poles, the self energy can be estimated from Eq. (26) as

$$\hat{\Sigma}_2^{(2)} \approx \frac{i\Delta}{4\pi v_F} \partial_E \hat{\Sigma}, \quad (27)$$

where we have used $m/|k_0| \approx 1/v_F$ and $\text{Tr}_{\vec{k}} \bar{G}(\vec{k}) = \hat{\Sigma}/\Delta$, see Eq. (23).

If we compare Eq. (27) to the corresponding second-order rainbow diagram, $\hat{\Sigma}_1^{(2)} = \hat{\Sigma}(-\partial_E \hat{\Sigma})$, we have

$$\left| \frac{\hat{\Sigma}_2^{(2)}}{\hat{\Sigma}_1^{(2)}} \right| \approx \frac{1}{4\pi\nu(E)/\nu_{1D}}. \quad (28)$$

Unless there is a gap for small E , this ratio is always smaller than $1/4\pi$. This is a conservative estimate since here we have neglected the real part $\hat{\Sigma}_R$ of the self energy, $\hat{\Sigma} = \hat{\Sigma}_R - i\pi\Delta\nu(E)$, see Eq. (24). Incorporating

it would simply decrease the ratio (28). Obviously, for high energies, i.e. high order n of the VHS, this NCA approach should become exact. Even for the lowest-order VHS, however, it is still expected to be quite accurate. We therefore conclude that our NCA-type treatment is highly accurate in describing disorder effects for the VHS in MWNTs. At this point it should be stressed that in the true 2D limit, our arguments leading to Eq. (28) are not valid, and therefore no contradiction to Refs. 14–18 arises.

V. RESULTS

We now deduce a formula that is appropriate for numerical evaluation. Inserting Eq. (15) into Eq. (23), we find by contour integration

$$\hat{\Sigma}(E) = -i\Delta \frac{\hbar v_F}{R} \sum_n \frac{(E - \hat{\Sigma}(E)) \text{sgn}(E - \hat{\Sigma}_R)}{\sqrt{(E - \hat{\Sigma}(E))^2 - E_n^2}}, \quad (29)$$

where correct units were restored for clarity, $E_n = \hbar v_F \omega_n$. This equation can easily be solved numerically. Once we know the self energy, we can compute the TDOS from Eq. (24),

$$\frac{\nu_{\text{bulk}}(E)}{\nu_{1D}} = \text{Re} \sum_n \frac{(E - \hat{\Sigma}(E)) \text{sgn}(E - \hat{\Sigma}_R)}{\sqrt{(E - \hat{\Sigma}(E))^2 - E_n^2}}. \quad (30)$$

The result (12) for the clean case is easily recovered in the limit $\Delta \rightarrow 0$. For $\Delta > 0$, the finite imaginary part of $\hat{\Sigma}$ in the denominator of (30) causes a broadening of the VHS, whereas the real part causes an energy shift of the peaks. Equations (29) and (30) can be used to fit experimental data for the TDOS of MWNTs. Assuming that R is known, since Δ is the only fit parameter, the disorder strength can then be determined directly from the TDOS. This would provide precious information on the disorder strength in the system.

For the numerical evaluation of Eq. (29), a cutoff for the summation over n has to be specified. Such a cutoff for the band index n is naturally given from the bandstructure. For instance, for armchair nanotubes, the number of subbands would be limited to $2N = 8\pi R/\sqrt{3}a$.²⁴ For $R = 10$ nm, $N \approx 295$, and in the figures below, we use this cutoff such that $n \in [-295, 295]$. The results are, however, not very sensitive to the precise choice of this cutoff.

As can be seen from Fig. 3, one effect of the disorder is a strong *broadening of the VHS*. For sufficiently strong disorder, the peaks can even disappear completely. The VHS, resulting from the opening of new subbands due to transverse momentum quantization, are destroyed once motion around the circumference becomes diffusive. When increasing Δ , van Hove peaks start to disappear at high energies. A further increase of the disorder strength then lowers the energy where the VHS vanish. In the

region where no VHS's are present, i.e. above a certain disorder-dependent energy threshold E_a , the TDOS behaves like a power law with a Δ -dependent exponent,

$$\nu(E) \sim E^\alpha, \quad (31)$$

with $\alpha = \alpha(\Delta) \leq 1$. Note that energies are absolute (not relative to E_F), and therefore this power law is unrelated to the findings of Ref. 13. This relation holds remarkably well for $\Delta \leq 0.05$. For $E < E_a$, instead of the power law (31), the TDOS approaches a finite value for $E \rightarrow 0$, see Fig. 4. We note that this power law has a different origin than the one found in the 2D case that rests upon the inclusion of crossed diagrams.¹⁴

In addition, the positions of the VHS's are *shifted to smaller energies* with increasing Δ . This shift grows approximately linearly with Δ , and the relative shift, compared to the position of the VHS in the clean system, can be up to 20%, depending on the disorder strength. Since the radius of a nanotube is often determined from the relative positions of the VHS, this observation suggests that such interpretations need to be taken with some caution. The disorder-induced shift has to be taken into account to obtain correct results. With decreasing radius and for increasing order n of the VHS, the relative shift becomes systematically smaller.

Next, if we consider a fixed disorder strength Δ and vary the strength of the magnetic field applied parallel to the tube axis, we find the situation depicted in Fig. 5. Again there is a doubling of the peaks corresponding to the VHS, and the shift of the positions varies periodically with the magnetic field. As in the clean case, there is a gap even in the presence of disorder. Due to the disorder-dependent shift of the VHS towards smaller energies, the gap gets partially filled with states and is therefore smaller than in the clean case. However, magnetic field effects are essentially not (or only weakly) affected by disorder.

Finally, we briefly turn to the boundary limit. Since it is easy to generalize Eqs. (29) and (30) to obtain the corresponding boundary TDOS, we only mention the modifications compared to the clean case. The disordered boundary TDOS is suppressed compared to the clean case and the suppression increases with increasing disorder strength. The positions of the van Hove nonanalyticities at the opening of new subbands are shifted to *higher* energies although the shift in the bulk case was to smaller energies. The form of the nonanalyticity is not significantly changed by the disorder but approximately retains a square-root energy dependence above the threshold.

VI. CONCLUSIONS AND OUTLOOK

We have calculated the TDOS of disordered multichannel quantum wires, with special emphasis on MWNTs. In the present theory, electron-electron interactions are

supposed to be screened off by a metallic substrate or a close-by gate. Focussing on potential scattering disorder, within a non-crossing approximation, a self-consistent non-perturbative summation of all diagrams for the self energy yields an analytical result for the disorder-broadened van Hove singularities in such a system. For given radius of the MWNT, our result involves only one parameter (the disorder strength Δ), which should allow for a detailed comparison to scanning tunneling spectroscopy experiments on MWNTs. We also stress that it is in general not possible to define an energy-independent mean free path for all energies.

Remarkably, the standard Born approximation breaks down in the vicinity of a van Hove singularity, and one has to include higher-order diagrams for the self energy. We have demonstrated that this problem can be approximately yet accurately solved by combining a non-crossing approximation with an iterative self-consistent summation of all remaining diagrams. The theory can then be applied to the energy dependence of the TDOS, and reveals remarkable differences in the bulk and boundary limits. These effects can easily be observed experimentally using available technology.

In the bulk limit, we observe broadened VHS's that are shifted to smaller energies compared to the clean case. For high energies, the TDOS behaves as a power law with energy, with a disorder-dependent exponent. In the boundary limit, VHS's appear only as nonanalyticities at the opening of new subbands, with a square-root energy dependence of the TDOS above the threshold. This behavior is basically unchanged in the disordered case, but we observed a shift of the nonanalyticities to higher energies and a disorder-dependent suppression of the TDOS.

ACKNOWLEDGMENTS

We thank A. O. Gogolin for useful discussions. Financial support by the DFG under the Gerhard-Hess program is acknowledged.

-
- ¹ L. van Hove, Phys. Rev. **89**, 1189 (1953).
 - ² J. Tersoff and D. R. Hamann, Phys. Rev. Lett. **50**, 1998 (1983); Phys. Rev. B **31**, 805 (1985).
 - ³ S. Hügler, R. Egger, and H. Grabert, Solid State Commun. **117**, 93 (2001).
 - ⁴ C. Dekker, Physics Today **52** (6), 22 (1999).
 - ⁵ S. J. Tans, M. H. Devoret, R. J. A. Groeneveld, and C. Dekker, Nature (London) **394**, 761 (1997).
 - ⁶ M. Bockrath, D. H. Cobden, J. Lu, A. G. Rinzler, R. E. Smalley, L. Balents, and P. L. McEuen, Nature (London) **397**, 598 (1999); Z. Yao, H. W. J. Postma, L. Balents, and C. Dekker, *ibid.* **402**, 273 (1999).

- ⁷ A. Bachtold, C. Strunk, J. P. Salvetat, J. M. Bonard, L. Forró, and C. Schöenberger, *Nature (London)* **397**, 673 (1999).
- ⁸ R. Egger and A. O. Gogolin, *Phys. Rev. Lett.* **87**, 66401 (2001).
- ⁹ S. Roche, F. Triozon, A. Rubio, and D. Mayou, *Phys. Rev. B* **64**, 121401(R) (2001).
- ¹⁰ J. W. G. Wildöer, L. C. Venema, A. G. Rinzler, R. E. Smalley, and C. Dekker, *Nature (London)* **391**, 59 (1998), T. W. Odom, J. L. Huang, P. Kim, and C. M. Lieber, *ibid.* **391**, 62 (1998).
- ¹¹ L. C. Venema, J. W. Janssen, M. R. Buitelaar, J. W. G. Wildöer, S. G. Lemay, L. P. Kouwenhoven, and C. Dekker, *Phys. Rev. B* **62**, 5238 (2000).
- ¹² P. Kim, T. W. Odom, J. -L. Huang, and C. M. Lieber, *Phys. Rev. Lett.* **82**, 1225 (1999).
- ¹³ A. Bachtold, M. de Jonge, K. Grove-Rasmussen, P. L. McEuen, M. Buitelaar, and C. Schöenberger, *Phys. Rev. Lett.* **87**, 166801 (2001). See also C. Schöenberger, A. Bachtold, C. Strunk, J. P. Salvetat, and L. Forró, *Appl. Phys. A* **69**, 283 (1999).
- ¹⁴ A. A. Nersisyan, A. M. Tsvelik, and F. Wenger, *Phys. Rev. Lett.* **72**, 2628 (1994); *Nucl. Phys. B* **438**, 561 (1995).
- ¹⁵ A. W. W. Ludwig, M. P. A. Fisher, R. Shankar, and G. Grinstein, *Phys. Rev. B* **50**, 7526 (1994).
- ¹⁶ C. Chamon, C. Mudry, and X. G. Wen, *Phys. Rev. Lett.* **77**, 4194 (1996); *Nucl. Phys. B* **466**, 383 (1996).
- ¹⁷ J. González, F. Guinea, and M. A. H. Vozmediano, *Phys. Rev. Lett.* **69**, 172 (1992); *Phys. Rev. B* **63**, 134421 (2001).
- ¹⁸ A. Altland, B. D. Simons, and M. R. Zirnbauer, preprint cond-mat/0006362.
- ¹⁹ D. P. DiVincenzo and E. J. Mele, *Phys. Rev. B* **29**, 1685 (1984).
- ²⁰ C. L. Kane and E. J. Mele, *Phys. Rev. Lett.* **78**, 1932 (1997).
- ²¹ J. W. Mintmire and C. T. White, *Phys. Rev. Lett.* **81**, 2506 (1998).
- ²² A. A. Abrikosov, L. P. Gorkov, and I. Dzyaloshinskii, *Quantum Field Theoretical Methods in Statistical Physics* (Pergamon, New York, 1965).
- ²³ P. A. Lee, *Phys. Rev. Lett.* **71**, 1887 (1993).
- ²⁴ R. A. Jishi, D. Inomata, K. Nakao, M. S. Dresselhaus, and G. Dresselhaus, *J. Phys. Soc. Jpn.* **63**, 2252 (1994).

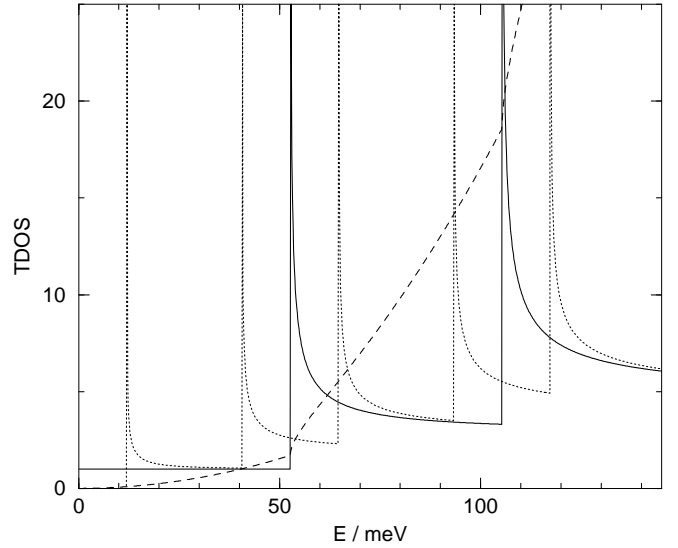


FIG. 1. Bulk and end TDOS of a clean tube. Without magnetic field the system is gapless and the bulk TDOS is finite for $E \rightarrow 0$ (solid curve). VHS's appear at the onset of new subbands. With magnetic field ($B = 3$ T), the system is gapped and the VHS's are doubled (dotted curve). The end TDOS (dashed curve) exhibits a square-root nonanalyticity instead of a divergence, and vanishes $\sim E^2$ for $E \rightarrow 0$. The scale for the end TDOS is arbitrary since it depends on the precise distance to the boundary.

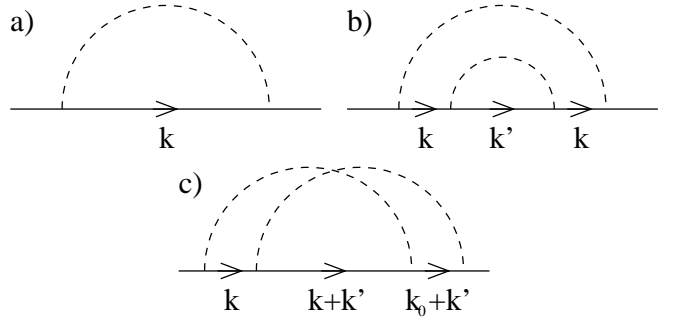


FIG. 2. First and second order self energy diagrams after disorder averaging. The solid line represents the bare propagator G_0 , while the dashed line represents the disorder potential scattering. In the vector model, each vertex contributes an additional factor σ_μ , where one has to sum over $\mu = x, y$. Compared to the crossed diagram c), the rainbow diagrams a) and b) have no dependence upon external momentum \vec{k}_0 .

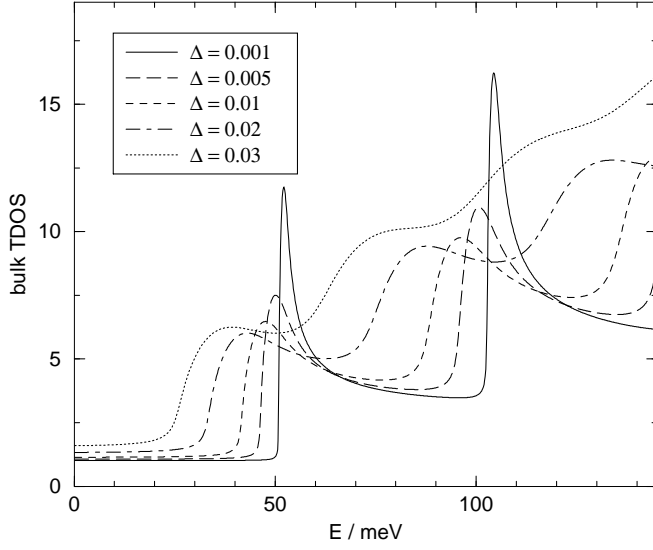


FIG. 3. Bulk TDOS of a disordered tube at $B = 0$ for different values of Δ . The broadening of the VHS with increasing Δ is clearly visible, as well as their shift towards smaller energies.

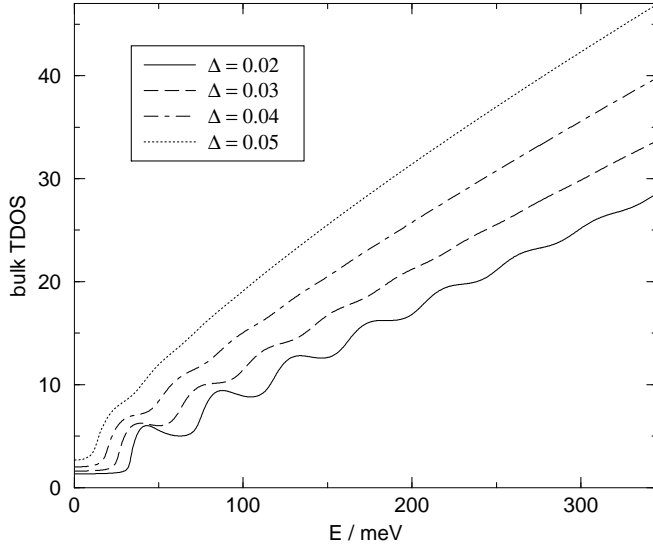


FIG. 4. Bulk TDOS of strongly disordered MWNTs at $B = 0$ for different Δ .

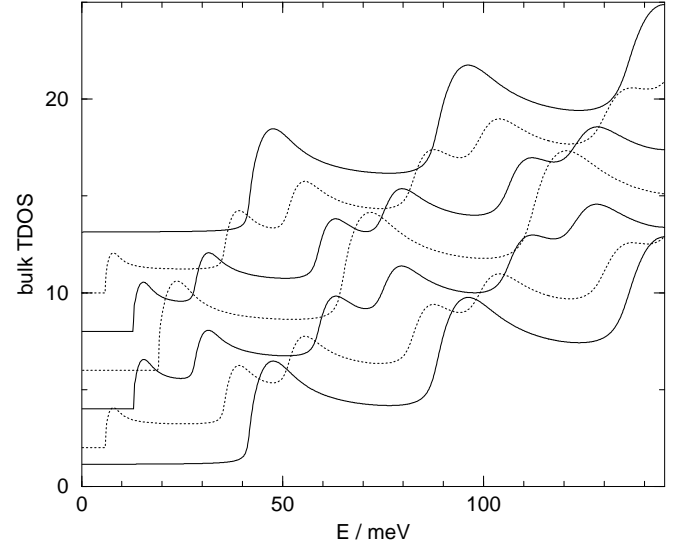


FIG. 5. Bulk TDOS for $\Delta = 0.01$ and different values of the magnetic field B . The curves corresponding to different B are shifted vertically by the same amount for better visibility. The lowest curve corresponds to $B = 0$, and then B increases in steps of $\Delta B = 2.2$ T. Notice the opening and closing of a gap with variation of B , and the periodicity in B with period $B_0 = 13.2$ T for $R = 10$ nm.